

NORTH-SOUTH NEUTRINO HEATING ASYMMETRY IN STRONGLY MAGNETIZED AND ROTATING STELLAR CORES

KEI KOTAKE,¹ SHOICHI YAMADA,² AND KATSUHIKO SATO^{1,3}

Received 2004 August 3; accepted 2004 September 6

ABSTRACT

We perform a series of magnetohydrodynamic simulations of supernova cores. Since the distributions of the angular momentum and the magnetic fields of strongly magnetized stars are quite uncertain, we systematically change the combinations of the strength of the angular momentum, rotation law, degree of differential rotation, and profiles of the magnetic fields to construct the initial conditions. By so doing, we estimate how the rotation-induced anisotropic neutrino heating is affected by the strong magnetic fields through parity-violating effects and for the first time investigate how the north-south asymmetry of the neutrino heating in a strongly magnetized supernova core could be affected. As for the microphysics, we employ a realistic equation of state based on the relativistic mean field theory and take into account electron captures and the neutrino transport via a neutrino leakage scheme. With these computations, we find that the neutrino heating rates are reduced by $\lesssim 0.5\%$ over those without the magnetic fields as a result of the parity-violating effects in the vicinity of the north pole of a star, while they are enhanced by about $\lesssim 0.5\%$ in the vicinity of the south pole. If the global asymmetry of the neutrino heating in the both of the poles develops in the later phases, the newly born neutron star might be kicked toward the north pole in the subsequent period.

Subject headings: neutrinos — pulsars: general — stars: magnetic fields — stars: rotation — supernovae: general

1. INTRODUCTION

Neutron stars are created in the aftermath of the gravitational core collapse of massive stars at the end of their lives. After the supernova explosions, the nascent neutron stars have rapid rotations and large magnetic fields and are believed to be observed as pulsars. Thus, rotations and magnetic fields naturally should be taken into account in order not only to clarify the explosion mechanism, but also to explain the observed properties of neutron stars. Here it is noted that the number of studies that include such multidimensional aspects has been increasing recently (Akiyama et al. 2003; Buras et al. 2003; Kotake et al. 2003a, 2003b, 2004b, 2004c; Ott et al. 2004; Yamada & Sawai 2004; Fryer & Warren 2004; Müller et al. 2004; Yamada et al. 2004). This may reflect the fact that it is difficult to produce a successful explosion only by means of a heating mechanism that assumes spherical symmetry (Rampp & Janka 2000; Liebendörfer et al. 2001, 2005; Thompson et al. 2003).

One of the unresolved mysteries in the context of core-collapse supernovae is the physical origin of the pulsar kicks, which has long been controversial. Recent analyses of individual pulsar motions and observations of remnant associations between supernovae and pulsars indicate that supernovae explosions are asymmetric and that neutron stars receive large kick velocities at birth (typically $300\text{--}400\text{ km s}^{-1}$ [Lyne & Lorimer 1994; Lorimer et al. 1997], with the highest values being greater than 1000 km s^{-1} [Arzoumanian et al. 2002]). The existence of pulsar kicks is also supported by evolutionary studies of neutron star and black hole binaries (Fryer & Kalogera 1997; Wex et al. 2000; Mirabel et al. 2002) and by detections of geodetic and orbital plane precessions in some binary pulsars

(Cordes et al. 1990; Kaspi et al. 1996). Recent X-ray observations have shown a correlation between the direction of pulsar motions and the spin axis of their supernovae in the Vela and Crab pulsars (Helfand et al. 2001; Pavlov et al. 2001). However, it is statistically uncertain whether the spin-kick alignment is a generic feature of all pulsars.

So far two major classes of mechanism for these kicks have been suggested (see Lai et al. 2001; Lai 2004 for a review). Any model or mechanism should explain how the explosions become asymmetric and how the generated asymmetric explosions are related to the formation of the pulsar kicks. The first class of mechanisms rely on asymmetric explosions resulting from global convective instabilities (Burrows & Hayes 1996; Goldreich et al. 1996) caused by the precollapse density inhomogeneities (Bazan & Arnett 1998) or the local convective instabilities (Janka & Mueller 1994) formed after the onset of core collapse. More recently, Scheck et al. (2004) reported that in their two-dimensional simulations, the neutrino-driven convections behind the expanding shock in long-duration explosions (more than a second after bounce) can lead to global asymmetries, which accelerates the remnant neutron star to a several hundreds of km s^{-1} (see also Fryer 2004 for three-dimensional calculations). In their simulations, the central proto-neutron star is fixed as the inner boundary condition. Fully self-consistent calculations are required to confirm whether this assumption is valid or not.

Here we pay attention to the second class of models, in which the pulsar kicks arise from an asymmetry of neutrinos induced by the strong magnetic field ($B \geq 10^{15}\text{ G}$) in the collapsed supernova core. While the dipolar magnetic fields of most radio pulsars are observed to lie in the range of $10^{12}\text{--}10^{13}\text{ G}$, several recent observations imply that the soft gamma-ray repeaters and anomalous X-ray pulsars have the strong magnetic fields as high as $B \sim 10^{15}\text{ G}$ (Zhang & Harding 2000; Guseinov et al. 2003). So far, much theoretical effort has been paid to formulate the neutrino opacity in such strong magnetic fields (Horowitz & Li 1998; Arras & Lai 1999a, 1999b). On the other hand, it

¹ Department of Physics, School of Science, University of Tokyo, 7-3-1 Hongo, Bunkyo, Tokyo 113-0033, Japan; kkotake@utap.phys.s.u-tokyo.ac.jp.

² Science & Engineering, Waseda University, 3-4-1 Okubo, Shinjyuku, Tokyo, 169-8555, Japan.

³ Research Center for the Early Universe, University of Tokyo, 7-3-1 Hongo, Bunkyo, Tokyo 113-0033, Japan.

seems that little attention has been paid to investigating on the basis of numerical simulations how asymmetric neutrino heating works globally in the supernova core. In addition, most of the preceding studies rely only on the asymmetry of the neutrinos caused by the magnetic fields (see, however, Janka & Raffelt [1999] and Duan & Qian [2004] for simple models of the atmosphere in the supernova core). We note that rotation should also contribute to producing the asymmetry of the neutrino heating (Kotake et al. 2003a). To our knowledge, the degree of the neutrino-heating asymmetry when rotation and strong magnetic fields are present at the same time has not been investigated so far. This situation leads us to investigate how rotation-induced anisotropic neutrino heating (Kotake et al. 2003a) is affected by strong magnetic fields through parity-violating effects. In this study, we perform a series of two-dimensional simulations of magnetorotational core collapse. In order to see the parity-violating effects, we pay particular attention to the models that are assumed to have strong poloidal magnetic fields ($\sim 10^{12}$ G) prior to core collapse. Since the profiles of the angular momentum and the magnetic fields of such strongly magnetized stars are still quite uncertain (see, however, Heger et al. 2003), we change the strength of the rotation and the magnetic fields systematically. On the basis of simulations from the onset of the core collapse through the bounce to the shock stall, we demonstrate how large the anisotropy of neutrino heating could be globally in the supernova core. Furthermore, we speculate about their possible effects on pulsar kicks.

We describe the numerical methods in § 2. The main numerical results are shown in § 3. Discussion is given in § 4. We conclude in § 5.

2. NUMERICAL METHODS AND INITIAL MODELS

The numerical method used for the magnetohydrodynamic (MHD) computations employed in this paper is based on the ZEUS-2D code (Stone & Norman 1992). ZEUS-2D is an Eulerian code based on the finite-difference method and employs the artificial viscosity of von Neumann and Richtmyer to capture shocks. The time evolution of the magnetic field is solved by an induction equation, $\partial \mathbf{B} / \partial t = \nabla \times (\mathbf{v} \times \mathbf{B})$, with \mathbf{v} and \mathbf{B} being the velocity and the magnetic field, respectively. In so doing, the code utilizes the so-called constrained transport (CT) method, which ensures that the numerically evolved magnetic fields are divergence-free ($\nabla \cdot \mathbf{B} = 0$) at all times. Furthermore, the method of characteristics (MOC) is implemented to propagate accurately all modes of the MHD waves. The self-gravity is managed by solving the Poisson equation with the incomplete Cholesky decomposition conjugate gradient method. In all the computations, spherical coordinates are used and one quadrant of the meridian section is covered with $300(r) \times 50(\theta)$ mesh points. We have made several major changes to the base code to incorporate the microphysics. First, we added an equation for the electron fraction to treat electron captures and neutrino transport by the so-called leakage scheme (Epstein & Pethick 1981; Bludman et al. 1982; van Riper & Lattimer 1981; van Riper 1982). The calculation of the electron fraction is done separately from the main hydrodynamic step in an operator-splitting manner. Second, we implemented a tabulated equation of state based on the relativistic mean field theory (Shen et al. 1998) instead of the ideal-gas equation of state assumed in the original code. For a more detailed description of the methods, see Kotake et al. (2003a).

2.1. Initial Conditions

Recently, Heger et al. (2003) performed up-to-date stellar evolution calculations that include the effects of rotation, mixing,

transport of the angular momentum, and the magnetic torques. Their models show that the toroidal magnetic fields are much stronger than the poloidal ones prior to core collapse. In our previous paper (Kotake et al. 2004b), we considered such models as the initial conditions. However, if such initial configurations are correct, no parity-violating effects of the magnetic fields on the neutrino heating can be obtained in two-dimensional axisymmetric simulations. Heger's models are one-dimensional, which hinders the accurate treatment of the transport of the angular momentum and the generation of the magnetic fields, but even considering the uncertainties in Heger's evolution calculations, it is still important to take poloidal magnetic fields as an initial condition. Thus, in this study, we assume that only the poloidal magnetic fields exist prior to core collapse and thus prefer a parametric approach to constructing the initial conditions, varying the profiles of the initial poloidal magnetic fields.

We assume the two rotation laws and four configurations of the magnetic fields:

1. Shell-type rotation,

$$\omega(r) = \omega_0 \frac{R_0^2}{r^2 + R_0^2}, \quad (1)$$

and shell-type magnetic fields,

$$B(r) = B_0 \frac{R_0^2}{r^2 + R_0^2}, \quad (2)$$

where $\omega(r)$ is an angular velocity, $B(r)$ is the poloidal component of the magnetic fields, r is radius, and ω_0 , R_0 , and B_0 are model constants.

2. Cylindrical rotation,

$$\omega(X, Z) = \omega_0 \left(\frac{X_0^2}{X^2 + X_0^2} \right) \left(\frac{Z_0^4}{Z^4 + Z_0^4} \right), \quad (3)$$

cylindrical magnetic fields,

$$B_z(X, Z) = B_0 \times \frac{X_0^2}{X^2 + X_0^2}, \quad (4)$$

and uniform cylindrical magnetic fields,

$$B_z = B_0, \quad (5)$$

where B_z is the poloidal magnetic field parallel to the rotational (Z) axis, X and Z denote distances from the rotational axis and the equatorial plane, and X_0 , Z_0 are model constants. The other parameters have the same meanings as above.

Finally, we take into account quadrupole magnetic fields following the prescription by Ardeljan et al. (1998):

$$\begin{aligned} B_x(X, Z) &= F_x(0.5\hat{X}, 0.5\hat{Z} - 2.5) - F_x(0.5\hat{X}, 0.5\hat{Z} + 2.5), \\ B_z(X, Z) &= F_z(0.5\hat{X}, 0.5\hat{Z} - 2.5) - F_z(0.5\hat{X}, 0.5\hat{Z} + 2.5), \end{aligned} \quad (6)$$

with

$$\hat{X} = \frac{X}{X_{0, \text{quad}}}, \quad \hat{Z} = \frac{Z}{Z_{0, \text{quad}}}, \quad (7)$$

TABLE 1
MODEL PARAMETERS

Model ^a	Rotation Profiles	B Profiles ^b	ω_0 (s^{-1})	B_0 (G)	$R_0, X_0, Z_0 \times 10^8$ (cm)
SL(U)-2	Shell	Uniform cylinder	0.6	1.9×10^{12}	$R_0 = 1$
SS(U)-2	Shell	Uniform cylinder	9.0	1.9×10^{12}	$R_0 = 0.1$
CS(U)-2	Cylinder	Uniform cylinder	6.3	1.9×10^{12}	$X_0 = 0.1, Z_0 = 1$
SS(NU)-2	Shell	Shell	9.0	1.1×10^{14}	$R_0 = 0.1$
CS(NU)-2	Cylinder	Cylinder	6.3	4.7×10^{13}	$X_0 = 0.1, Z_0 = 1$
SL(Q)-2	Shell	Quadrupole	9.0	1.4×10^{13}	$R_0 = 1, X_{0, \text{quad}} = Z_{0, \text{quad}} = 1.6$
CS(Q)-2	Cylinder	Quadrupole	6.3	1.4×10^{13}	$X_0 = 0.1, Z_0 = 1, X_{0, \text{quad}} = Z_{0, \text{quad}} = 1.6$
SL(U)-1	Shell	Uniform cylinder	1.7	1.9×10^{12}	$R_0 = 1$
SS(U)-1	Shell	Uniform cylinder	28.3	1.9×10^{12}	$R_0 = 0.1$
SL(NU)-1	Shell	Shell	1.7	5.2×10^{12}	$R_0 = 1$
SS(NU)-1	Shell	Shell	28.3	1.1×10^{14}	$R_0 = 0.1$

^a The number (1 or 2) that each model has in its name indicates values of initial $T/|W|$ of 0.1% and 0.01%, respectively.

^b Profiles of the initial magnetic fields.

and

$$\begin{aligned}
 F_x(\hat{X}, \hat{Z}) &= B_0 \left[\frac{2\hat{X}\hat{Z}}{(\hat{Z}^2 + 1)^3} - \frac{2\hat{X}^3\hat{Z}}{(\hat{Z}^2 + 1)^5} \right], \\
 F_z(\hat{X}, \hat{Z}) &= B_0 \left[\frac{1}{(\hat{Z}^2 + 1)^2} - \frac{\hat{X}^2}{(\hat{Z}^2 + 1)^4} \right], \quad (8)
 \end{aligned}$$

where B_x is the poloidal magnetic fields parallel to the equatorial plane and $X_{0, \text{quad}}, Z_{0, \text{quad}}$ are model constants.

We have computed 11 models, changing the combination of the strength of the angular momentum, the rotation law, the degree of differential rotation, and the profiles of the magnetic fields. For all the models, we fix the values of $E_m/|W|$ to be 0.1%, where $E_m/|W|$ represents the ratio of magnetic to gravitational energy. The model parameters are presented in Table 1. The models are named after this combination. The first letter, S (shell) or C (cylindrical), denotes the rotation profile; the second letter, L (long) or S (short), indicates the values of R_0 and X_0 ; the letters in parentheses, U (uniform), NU (nonuniform), or Q (quadrupole) indicate the configurations of the initial poloidal magnetic field; and the numbers at the end, 1 or 2, indicate whether the initial $T/|W|$ is $10^{-1}\%$ or $10^{-2}\%$, respectively. Note that the ratio of rotational to gravitational energy is designated as $T/|W|$.

We note that our choice of the initial value of $T/|W|$ is much smaller than that of the past magnetorotational studies in the context of core-collapse supernovae (LeBlanc & Wilson 1970; Bisnovatyi-Kogan et al. 1976; Müller & Hillebrandt 1979; Symbalisty 1984; Ardeljan et al. 2000), to reconcile with the recent stellar evolution calculations of rotating stars (Heger et al. 2000). However, it is still larger than that of the slowest rotating models predicted by the most recent stellar calculations (Heger et al. 2003).

As for the configurations of the initial magnetic fields, we prepared a variety of them in order to cover as wide the parametric space of the field configurations as possible. As for the initial strength of the magnetic fields, we pay particular attention to the models, which are assumed to have the strong poloidal magnetic fields ($\sim 10^{12}$ G) prior to core collapse in order to see the parity-violating effects. Astrophysically, such models are likely to be associated with the formation of the so-called magnetars.

3. RESULTS

3.1. Magnetohydrodynamic Features

We briefly summarize some dynamical aspects that will be helpful in the later discussions. For the more detailed magnetohydrodynamic computations during core collapse, see also our accompanying paper (Takiwaki et al. 2004).

In Figure 1 the entropy distributions at the final states for some representative models are presented. The final time of all the models is about 50 ms after core bounce (see Table 2). At the final time, the shock wave produced at core bounce tends to stall in the core, except for the models that have centrally condensed magnetic fields and rapid rotation with strong differential rotation initially [see Fig. 1 and Table 2 for models CS(NU)-2, SS(U)-1, and SS(NU)-1]. Even if the shock waves of such models manage to approach the outer boundary of the numerical simulation ($Z \sim 1500$ km) along the rotational axis, the explosion energy is about 1 order of magnitude less than the canonical one. Thus, neutrino heating in the later phases is necessary for successful explosions. We note that the final values of $T/|W|$ and $E_m/|W|$ for our models are well below those of previous MHD studies (Symbalisty 1984), which assume rapid rotation prior to core collapse. Even in our models, which have slower rotation than the previous simulations, asymmetric matter motions can appear, as seen from Figure 1.

During core collapse, the strength of the magnetic fields exceeds the critical value $B_{\text{QED}} = 4.4 \times 10^{13}$ G, above which the neutrino reactions are affected by the parity-violating corrections of weak interactions. Just before core bounce, the poloidal magnetic fields dominate over the toroidal ones because of our assumption of the initial field configuration. After core bounce, the strong differential rotations near the surface of the proto-neutron star wrap the poloidal magnetic fields and convert them into toroidal ones whose strength becomes as high as $B \sim 10^{15}$ G at the final time of the simulations. The growth of the toroidal magnetic fields can be estimated by an order-of-magnitude estimate as follows:

$$B_\phi \sim 2.0 \times 10^{15} \text{ G} \left(\frac{B_z}{10^{15} \text{ G}} \right) \left(\frac{\Delta t}{50 \text{ ms}} \right) \left(\frac{\omega}{500 \text{ rad s}^{-1}} \right), \quad (9)$$

where B_z is the typical strength of the magnetic field parallel to the rotational axis just before core bounce; Δt is the duration of the wrapping time, which is roughly equivalent to the time

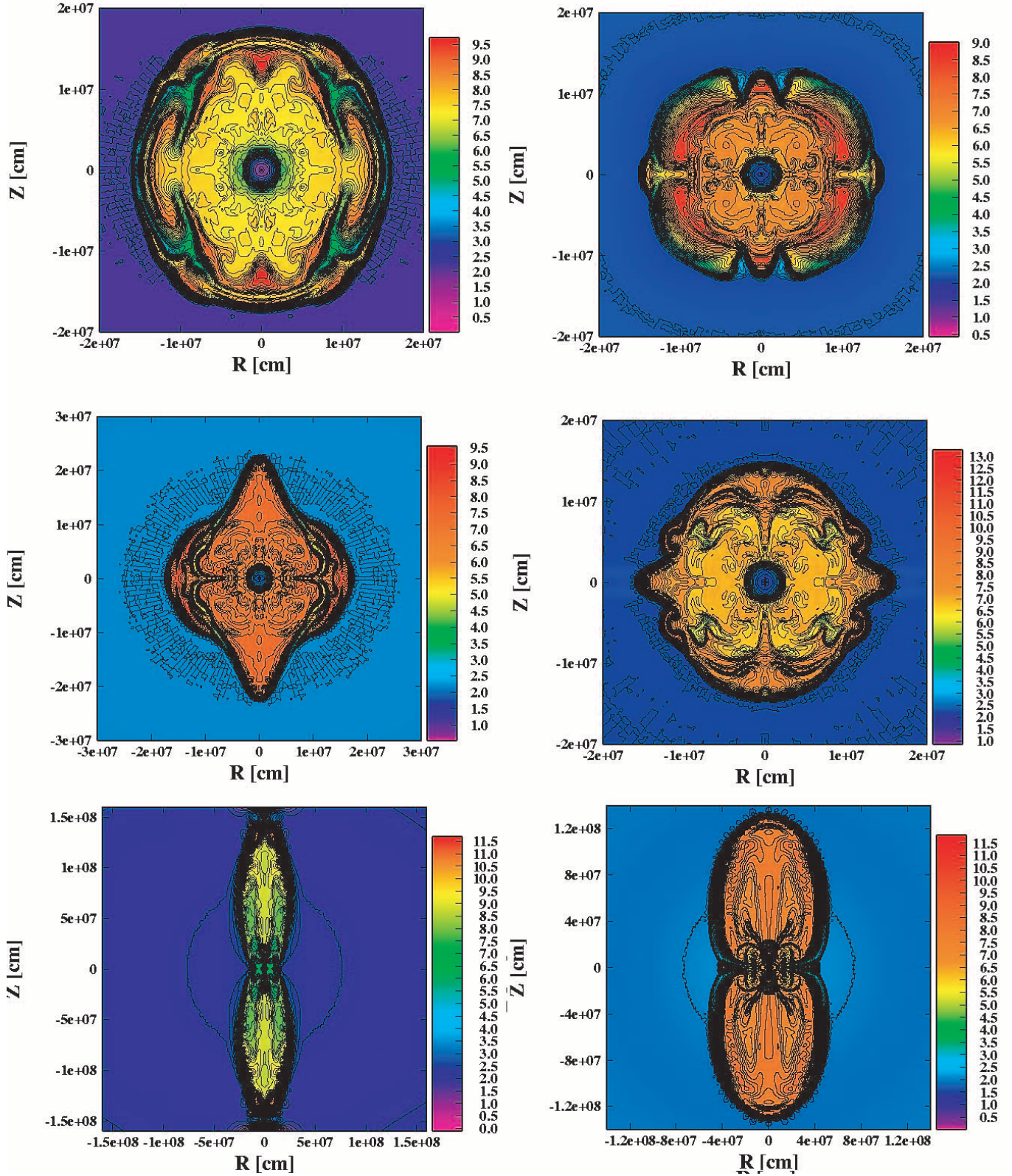


FIG. 1.—Final profiles of models SL(U)-2 (*top left*), SS(Q)-2 (*top right*), SS(U)-2 (*middle left*), SS(NU)-2 (*middle right*), CS(NU)-2 (*bottom left*), and SS(NU)-1 (*bottom right*), showing color-coded contour plots of entropy (in units of k_B) per nucleon.

from core bounce to the final time; and ω is the mean angular velocity at the surface of the proto-neutron star. This estimate is roughly consistent with the numerical simulations. We note that the tangled toroidal magnetic fields ($B_\phi \lesssim 10^{16}$ G) are weaker than the poloidal ones ($B_p \gtrsim 10^{16}$ G) at the final time in our

models (see Table 2). Magnetorotational instability (MRI) is another candidate for amplifying the growth of the toroidal magnetic fields. Although the typical timescale (Balbus & Hawley 1998) corresponding to the maximum growth of MRI [$\tau_{\text{MRI}} \sim O(10)$ ms] at the surface of the proto-neutron star is shorter than

TABLE 2
PROPERTIES OF THE FINAL STATES

Model	t_f (ms)	B_p (G)	B_ϕ (G)	r_{sh}^e (km)	r_{sh}^p (km)	$T/ W _f$ (%)	$E_m/ W _f$ (%)
SL(U)-2.....	40.2	1.5×10^{16}	2.4×10^{15}	157	175	2.5×10^{-1}	1.9×10^{-1}
SS(U)-2.....	41.8	3.4×10^{16}	2.3×10^{15}	178	233	2.5×10^{-1}	1.7×10^{-1}
CS(U)-2.....	40.7	3.2×10^{16}	3.7×10^{15}	144	612	2.5×10^{-1}	1.7×10^{-1}
SS(NU)-2.....	42.5	5.2×10^{16}	1.9×10^{15}	163	148	1.1×10^{-1}	5.3×10^{-1}
CS(NU)-2.....	43.1	4.6×10^{16}	4.9×10^{14}	176	1471	1.1×10^{-1}	3.7×10^{-1}
SL(Q)-2.....	37.1	1.2×10^{16}	9.4×10^{15}	146	125	2.6×10^{-1}	5.2×10^{-2}
CS(Q)-2.....	46.0	3.0×10^{16}	9.3×10^{15}	169	215	3.4×10^{-1}	7.1×10^{-2}
SL(U)-1.....	42.3	3.0×10^{16}	6.0×10^{15}	226	573	1.4	3.8×10^{-1}
SS(U)-1.....	47.1	4.1×10^{16}	2.0×10^{16}	133	1361	1.8	3.6×10^{-1}
SL(NU)-1.....	45.0	2.7×10^{16}	4.9×10^{15}	278	444	1.0	8.3×10^{-1}
SS(NU)-1.....	44.4	5.8×10^{16}	7.0×10^{14}	425	1325	2.8×10^{-1}	8.6×10^{-1}

NOTE.—Values of t_f represent the final time measured from core bounce; B_p and B_ϕ are the maximum strength of the poloidal and the toroidal magnetic fields, respectively; and r_{sh}^e and r_{sh}^p are the distances from the center to the stalled shock front in the equatorial plane and along the rotational axis, respectively.

the simulation timescale (~ 50 ms), it is much longer than the growth timescale of the field wrapping [$\tau_{wrap} \sim O(1)$ ms]. Thus the amplification of the toroidal magnetic fields in our models is mainly a result of the winding up of the original vertical poloidal fields.

In Figure 2 the cumulative distribution of specific angular momentum is shown for models CS(U)-2 and CS(NU)-2. In the magnetorotational core collapse, the anisotropic magnetic stress transfers the specific angular momentum of each fluid element outward even in axisymmetry if the fluid rotates differentially. We note that the mass of the unshocked core is about $\sim 0.8 M_\odot$ in these models. From the figure, we find that the transport of the angular momentum occurs more efficiently for model CS(NU)-2, whose initial magnetic fields are more centrally condensed, than for model CS(U)-2 (compare the specific angular momentum in Fig. 2). In addition, there are regions just outside the unshocked core where the specific angular momentum decreases outward. In such regions, the so-called Rayleigh instability condition holds, which induces the convection at the later phases near the surface of the unshocked core in the equatorial plane. The differences mentioned above stem only from the degree of

initial concentration of the magnetic fields between the pair of models and are common to the other pairs of models.

After the final time of our simulations, we calculate the shapes of the neutrino spheres by prescription (Kotake et al. 2003a). Although the magnetic fields become as strong as $B \sim 10^{15}$ G in the vicinity of the neutrino sphere ($r = 50\text{--}70$ km, density $\sim 10^{11}$ g cm $^{-3}$), the pressure of the magnetic fields [$p_{mag} \equiv B^2/8\pi \sim 10^{29}(B/2 \times 10^{15} \text{ G})^2$ dyn cm $^{-2}$] is smaller than that of the matter ($p_{matter} \sim 10^{30}$ dyn cm $^{-2}$) in the corresponding region (see Fig. 3, *left panel*). Thus it is found that the magnetic fields do not affect the shape of the neutrino sphere significantly. In fact, the neutrino spheres are deformed and become oblate for the rapidly rotating models, but on the other hand, become rather spherical for the slowly rotating models [see the right panel of Fig. 3 and compare the shape of the neutrino sphere of model SS(NU)-1 (the fastest rotating model in our computation) with that of the other (slower rotating) models].

3.2. Effects of the Strong Magnetic Fields on the Neutrino Heating

On the basis of the neutrino spheres obtained in the previous section, we estimate the heating rates, including the corrections from the parity-violating effects outside the neutrino sphere. This will admittedly be a very crude estimate, since it has been pointed out (Liebendörfer et al. 2001; Thompson et al. 2003) that the net heating (the heating minus cooling), becomes positive $\sim 50\text{--}100$ ms after the shock stagnation. In this respect, we confirmed that the cooling also dominates over the heating for our models that include corrections for the parity-violating effects. Since our calculations ended before the heating dominates over the cooling, it is impossible to estimate the location of the gain radius, beyond which the heating dominates over the cooling. Here we note that the contrast of the heating to the cooling is found to be similar in our short simulation runs. Thus, the gain radius should also be deformed in the later phase. If this feature lasts in the later phase, the bare heating rate discussed below and the resultant neutrino asymmetry due to the parity-violating corrections will help us understand the net neutrino asymmetry. Hence, bearing this caveat in mind, we study the bare heating rate with the parity-violating effects for the final configurations (several tens of milliseconds after the bounce) in our simulations.

First of all, we state how we estimate the neutrino heating rate in the strongly magnetized supernova core. The analysis scheme

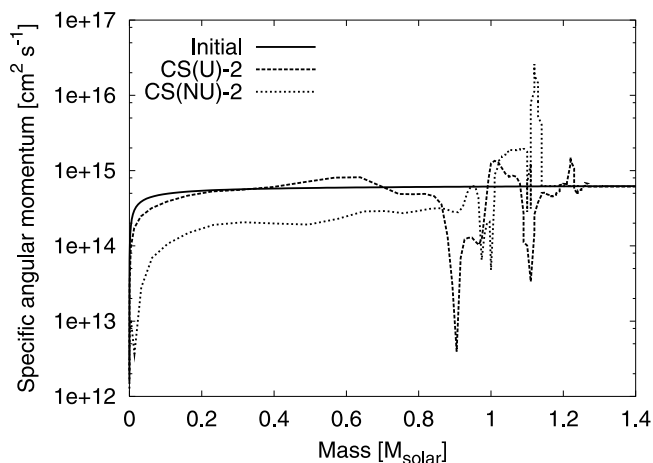


FIG. 2.—Cumulative mass vs. specific angular momentum distribution in units of M_\odot for models CS(U)-2 and CS(NU)-2 at the final state. Note that in the figure “Initial” represents the initial configuration of the specific angular momentum for the models. It is seen that the angular momentum is transferred more efficiently for the model with the centrally condensed magnetic fields profile [model CS(NU)-2] than for model CS(U)-2.

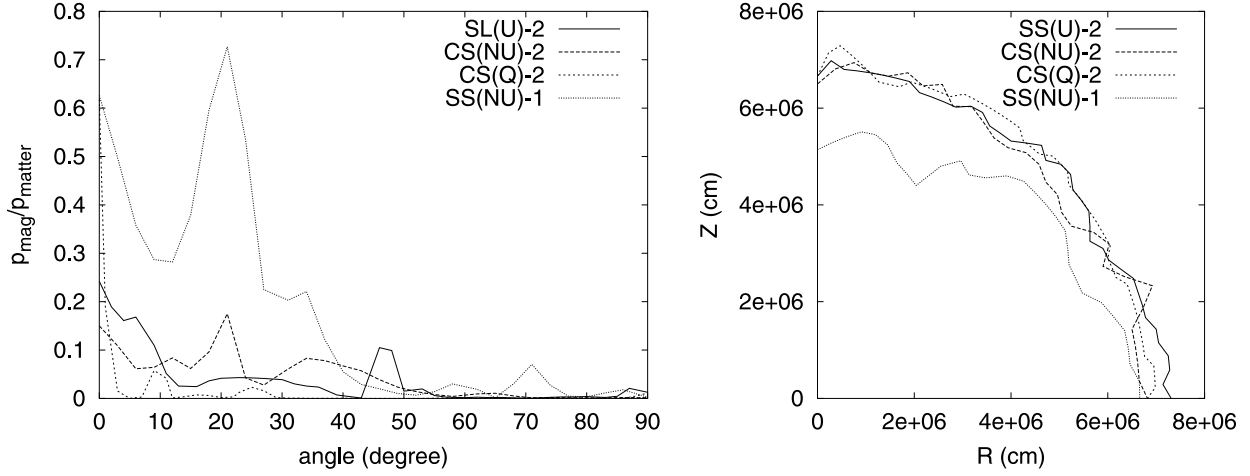


FIG. 3.—Ratio of the magnetic (p_{mag}) to the matter pressure (p_{matter}) with the polar angle on the neutrino sphere (*left panel*) and the shapes of the neutrino spheres for some representative models (*right panel*). Note in the right panel that R and Z represent the distances from the rotational axis and the equatorial plane, respectively.

is schematically shown in Figure 4. Neutrinos are assumed to be emitted isotropically from each point on the neutrino sphere and stream freely later on. Then the heating rate at a given point outside the neutrino sphere can be found by summing up all the rays from the neutrino sphere.

The heating by electron neutrinos proceeds via the charged current interaction:

$$\nu_e + n \rightarrow p + e^- . \quad (10)$$

We employ the corresponding cross section in a strongly magnetic field given by Arras & Lai (1999a), which is expressed as

$$\sigma_B^{(\text{abs})} = \sigma_0^{(\text{abs})} (1 + \epsilon_{\text{abs}} \hat{\mathbf{n}} \cdot \hat{\mathbf{B}}), \quad (11)$$

where $\sigma_0^{(\text{abs})}$ is the corresponding cross section without the magnetic fields, $\hat{\mathbf{n}}$ and $\hat{\mathbf{B}}$ are the unit momentum vector for the

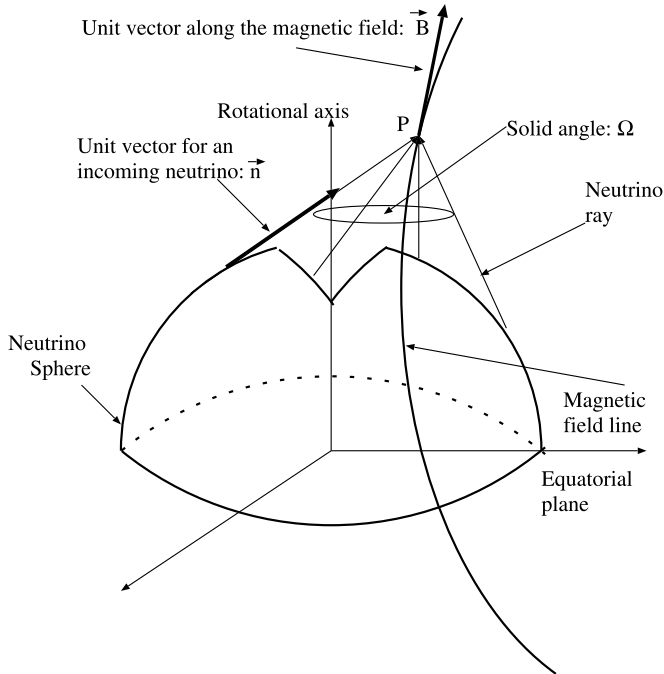


FIG. 4.—Schematic drawing of the analysis scheme of the heating rate. Neutrinos are assumed to be emitted isotropically from each point on the neutrino sphere. The heating rate at P can be found by summing up the contributions of all rays reaching P .

incoming neutrinos and the unit vector along the magnetic field direction (see Fig. 4), and ϵ_{abs} is the asymmetry parameter given by

$$\epsilon_{\text{abs}} = \epsilon_{\text{abs}}(e) + \epsilon_{\text{abs}}(n, n). \quad (12)$$

Here $\epsilon_{\text{abs}}(e)$ and $\epsilon_{\text{abs}}(np)$ are expressed in the leading order at the neutrino energies as

$$\epsilon_{\text{abs}}(e) = \frac{1}{2} \left(\frac{\hbar c e B}{\epsilon_\nu^2} \right) \left(\frac{c_V^2 - c_A^2}{c_V^2 + 3c_A^2} \right), \quad (13)$$

and

$$\begin{aligned} \epsilon_{\text{abs}}(n, p) = & 2 \frac{c_A(c_A + c_V)}{c_V^2 + 3c_A^2} \frac{\mu_{Bn} B}{k_B T} - \frac{k_B T}{\epsilon_\nu} \left(1 + \frac{\epsilon_\nu}{k_B T} \right) \\ & \times \left[2 \frac{c_A(c_A + c_V)}{c_V^2 + 3c_A^2} \frac{\mu_{Bn} B}{k_B T} + 2 \frac{c_A(c_A - c_V)}{c_V^2 + 3c_A^2} \frac{\mu_{Bp} B}{k_B T} \right], \end{aligned} \quad (14)$$

which represent the effects of electron Landau levels in magnetic fields and the polarizations of neutrons and protons, respectively. Here k_B is the Boltzmann constant, $\mu_{Bn} = -1.913\mu_N$, $\mu_{Bp} = 2.793\mu_N$ are the magnetic moments of neutrons and protons, respectively, with μ_N being the nuclear magneton, $c_V = 1$, $c_A = 1.26$ are the coupling constants. At the considered densities and temperatures, fermion phase space blocking and dense-medium effects can be safely ignored. The heating rate is given as

$$Q_\nu^+ = \int \sigma_B^{(\text{abs})} c n_{\text{neutron}} \epsilon_\nu \frac{d^2 n_\nu}{d\epsilon_\nu d\Omega} d\epsilon_\nu d\Omega, \quad (15)$$

where n_{neutron} is the number density of neutron and $d^2 n_\nu / (d\epsilon_\nu d\Omega)$ is related to the neutrino distribution in the phase space $f(\epsilon_\nu, \Omega)$:

$$\frac{d^2 n_\nu}{d\epsilon_\nu d\Omega} = \frac{1}{(hc)^3} f_\nu(\epsilon_\nu, \Omega) \epsilon_\nu^2. \quad (16)$$

Introducing equation (16) into equation (15) yields

$$Q_\nu^+ = \frac{c n_{\text{neutron}}}{(hc)^3} \int \sigma_B^{(\text{abs})} \epsilon_\nu^3 f_\nu(\epsilon_\nu, \Omega) d\Omega d\epsilon_\nu. \quad (17)$$

Introducing equation (11) into equation (17) yields

$$\begin{aligned} Q_\nu^+ &= \frac{cn_{\text{neutron}}}{(hc)^3} \int \sigma_0^{(\text{abs})} \epsilon_\nu^3 f_\nu(\epsilon_\nu, \Omega) d\Omega d\epsilon_\nu \\ &+ \frac{cn_{\text{neutron}}}{(hc)^3} \int \sigma_0^{(\text{abs})} \epsilon_{\text{abs}} \hat{\mathbf{n}} \cdot \hat{\mathbf{B}} \epsilon_\nu^3 f_\nu(\epsilon_\nu, \Omega) d\Omega d\epsilon_\nu \\ &\equiv Q_{\nu, B=0}^+ + \Delta Q_{\nu, B \neq 0}^+. \end{aligned} \quad (18)$$

The first term in equation (18) can be expressed as

$$Q_{\nu, B=0}^+ = \frac{3c_A^2 + 1}{4} \frac{\sigma_0 cn_{\text{neutron}}}{(hc)^3} \frac{\langle \epsilon_\nu^2 \rangle}{(m_e c^2)^2} \Omega \int d\epsilon_\nu \epsilon_\nu^3 f_\nu(\epsilon_\nu), \quad (19)$$

where

$$\langle \epsilon_\nu^2 \rangle = \int d\epsilon_\nu \epsilon_\nu^5 f_\nu(\epsilon_\nu) \left[\int d\epsilon_\nu \epsilon_\nu^3 f_\nu(\epsilon_\nu) \right]^{-1}. \quad (20)$$

Here Ω is the solid angle, within which a point outside the neutrino sphere can receive the neutrinos. It is calculated by the geometric calculations (see Fig. 4). As stated, the neutrino emission from each point on the neutrino sphere is assumed to be isotropic and take a Fermi distribution with a vanishing chemical potential. Equation (19) is expressed with the local neutrino flux, j_ν , which is in turn fixed from the neutrino luminosity obtained in the simulations:

$$Q_{\nu, B=0}^+ = \frac{(3c_A^2 + 1)}{4\pi} \sigma_0 n_{\text{neutron}} \frac{[F_5(0)/F_3(0)](kT_\nu)^2}{(m_e c^2)^2} j_\nu \Omega, \quad (21)$$

where we used the relations,

$$\langle \epsilon_\nu^2 \rangle = F_5(0)/F_3(0)(kT_\nu)^2, \quad (22)$$

with $F_5(0)$ and $F_3(0)$ being the Fermi integrals and

$$\begin{aligned} j_\nu &= c \frac{2\pi}{(hc)^3} \int d\epsilon_\nu \epsilon_\nu^3 f_\nu(\epsilon_\nu) \int_0^1 d\mu \mu \\ &= c \frac{\pi}{(hc)^3} \int d\epsilon_\nu \epsilon_\nu^3 f_\nu(\epsilon_\nu). \end{aligned} \quad (23)$$

By the same procedure as above, the heating rate arising from the parity violating effects can be given as follows,

$$\begin{aligned} \Delta Q_{\nu, B \neq 0}^+ &= \frac{3c_A^2 + 1}{4\pi} \sigma_0 n_{\text{neutron}} \left\{ \left(\int d\Omega \hat{\mathbf{n}} \cdot \hat{\mathbf{B}} \right) \frac{1}{(m_e c^2)^2} \right. \\ &\times \left[\frac{1}{2} \hbar c e B \frac{c_V^2 - c_A^2}{c_V^2 + 3c_A^2} - 2 \frac{c_A(c_A + c_V)}{c_V^2 + 3c_A^2} \frac{F_4(0)}{F_3(0)} (\mu_{Bn} B)(k_B T_\nu) \right. \\ &- 2 \frac{c_A(c_A - c_V)}{c_V^2 + 3c_A^2} \frac{\mu_{Bp} B}{k_B T} \frac{F_5(0)}{F_3(0)} (k_B T_\nu)^2 \\ &\left. \left. - 2 \frac{c_A(c_A - c_V)}{c_V^2 + 3c_A^2} \frac{F_4(0)}{F_3(0)} (\mu_{Bp} B)(k_B T_\nu) \right] j_\nu \right\}. \end{aligned} \quad (24)$$

Here $F_4(0)$ is the Fermi integral. The inner product of $\hat{\mathbf{n}} \cdot \hat{\mathbf{B}}$ can be obtained at each point by the geometry.

Using the hydrodynamic quantities at the final time of the numerical simulations (~ 50 ms) as a background, we demonstrate how much the rotation-induced anisotropic neutrino heating can be affected by the parity-violating corrections in the following.

First of all, we take the model SS(U)-2 as an example model. The configuration of the poloidal magnetic fields at the final state is presented in the top left panel of Figure 5. This panel shows that the poloidal magnetic fields are rather straight and parallel to the rotational axis in the regions near the rotational axis, but that, on the other hand, they are bent in a complex manner in the other central regions. This can be understood as follows. The core bounce occurs anisotropically owing to rotation. This induces convective motions. The magnetic fields are bent by the convective motions because the magnetic fields are frozen in fluid elements. This is because the ideal MHD is assumed in our simulations. The top right panel of Figure 5 shows the ratio of the neutrino heating rate corrected for parity-violating effects, $\Delta Q_{\nu, B \neq 0}^+$ to the heating rate without the corrections, $Q_{\nu, B=0}^+$. Note in the panel that the values of the color scale are expressed as percentages and that the central black region represents the region inside the neutrino sphere. It should be remembered that we took the two choices of $T/|W|$ as the initial condition. In the models with the smaller $T/|W| = 0.01\%$, the shapes of the neutrino sphere are found to be rather spherical and the resultant neutrino heating from the neutrino sphere becomes almost isotropic (see the models whose names end with “-2” in the right panel of Fig. 3 and Table 3). In such models, it is found that the initial rotation rate and magnetic field are not large enough to make the shapes of the neutrino sphere deviated from being spherically symmetric as in case of the pure rotation (Kotake et al. 2003a). In the top right panel, it is seen that the values of the ratio become negative in almost all the regions (for clarity, see also Fig. 5, *bottom right panel*). This means that the heating rate is more reduced with the magnetic fields than that without. In particular, this tendency is most remarkable in the regions near the rotational axis and the surface of the neutrino sphere (see the blue regions in the top right panel of Fig. 5). These features can be understood as follows. Let us remember that the first term in equation (24) represents the electron contribution arising from the ground Landau level, and the other represents the contribution from the neutron and proton polarizations. By an order-of-magnitude estimation, it can be readily found that the first term dominates over the other in the central core, with typical values of $B \geq 10^{15}$ G, $T \sim O(\text{MeV})$. Since the coefficient of the first term, which is proportional to the coupling constants of weak interactions ($\propto c_V^2 - c_A^2$, where $c_V = 1$, $c_A = 1.26$) is always negative, then the suppression or enhancement of the heating rate through parity-violating effects is determined by the signs of the inner product of $\hat{\mathbf{n}} \cdot \hat{\mathbf{B}}$. As mentioned above, the magnetic fields are almost aligned and parallel to the rotational axis in the regions near the rotational axis. With the rather spherical neutrino emission, the values of the inner product become positive in these regions, which results in a reduction of the heating rate. On the other hand, the values of the ratio become positive in some regions, where the poloidal magnetic fields are bent as a result of convections (see the red and white regions in the top and bottom right panels of Fig. 5, respectively). In fact, the contributions of the inner product are negative in such regions. In the bottom left panel of Figure 5, the contour of the ratio in the 360 latitudinal degree region of a star is prepared in order to see the global asymmetry of the heating. Since our simulations assume equatorial symmetry, the above features in the northern part of the star are reversed for the southern part. These features of the global asymmetry of the neutrino heating rates are common to most of the other models. In the following, we state some important features of the global asymmetry produced by the difference of the initial rotation rate or the initial configurations of the magnetic fields.

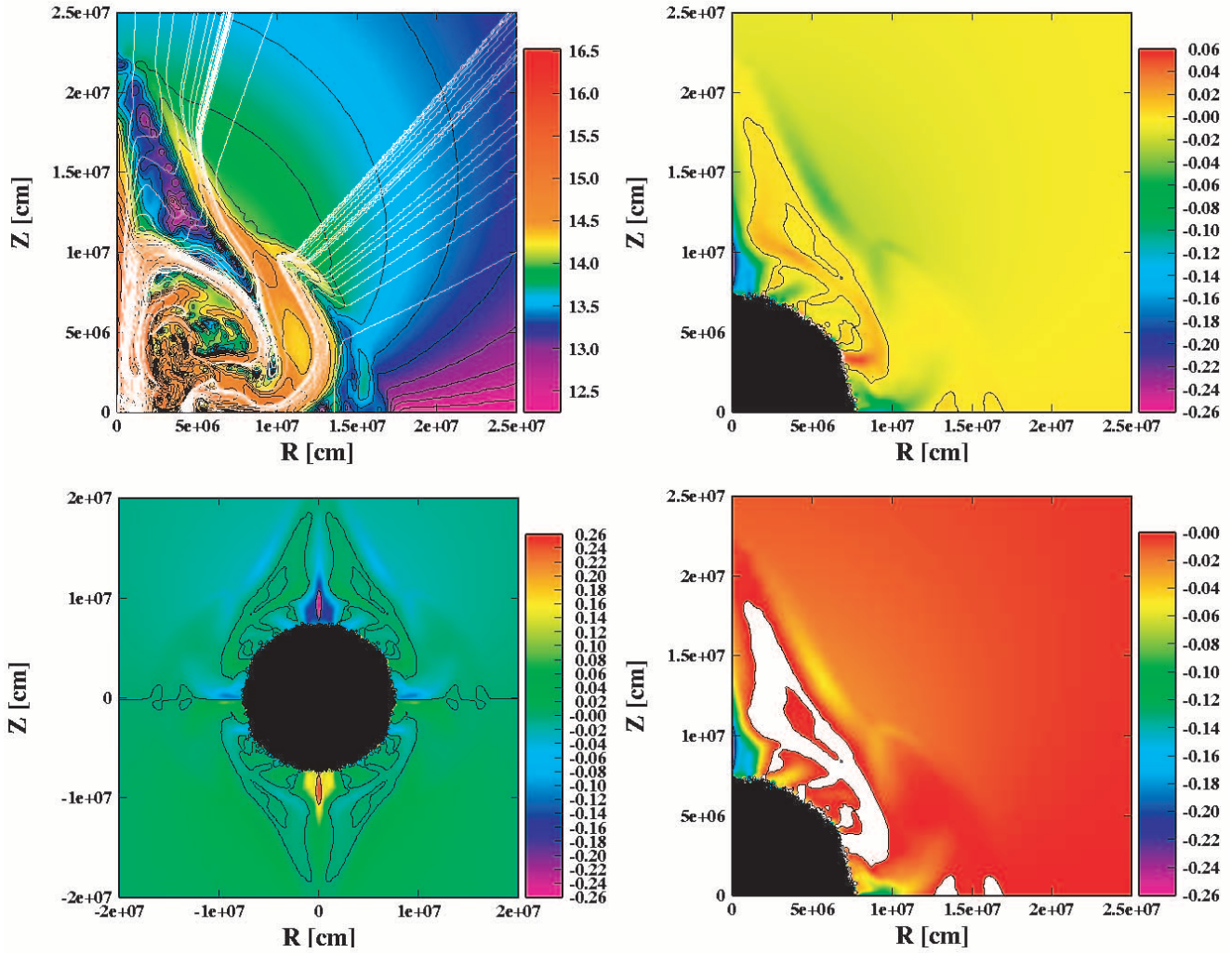


FIG. 5.—Various quantities for model SSU-2. *Top left*: Contour of the logarithm of the poloidal magnetic fields [$\log [B_p \text{ (G)}]$] with the magnetic field lines. *Top right*: Ratio of the neutrino heating rate corrected from the parity-violating effects, $\Delta Q_{\nu, B \neq 0}^+$, to the heating rate without the corrections, $Q_{\nu, B=0}^+$. Note in the panel that the values of the color scale are expressed in percentages and that the central black region represents the region inside the neutrino sphere. *Bottom right*: Same as the top right, but showing only the regions with negative values of the ratio. Thus, the white region shows the regions with positive values of the ratio. *Bottom left*: Contour of the ratio in the whole region, which shows the global asymmetry of the heating induced by the strong magnetic fields.

TABLE 3
ANALYSIS OF THE HEATING RATE
IN THE STRONG MAGNETIC FIELDS

Model	R_{ν}^p (km)	R_{ν}^e (km)	R_{mag} (%)
SL(U)-2	66.6	73.1	0.13
SS(U)-2	71.4	71.4	0.27
CS(U)-2	57.3	73.1	0.27
SS(NU)-2	65.1	68.2	0.08
CS(NU)-2	54.3	68.2	0.18
SL(Q)-2	69.8	68.2	0.14
CS(Q)-2	66.6	68.2	0.09
SL(U)-1	57.3	73.1	0.37
SS(U)-1	55.8	66.6	0.42
SL(NU)-1	50.0	65.1	0.26
SS(NU)-1	51.4	66.6	0.12

NOTES.— R_{ν}^e and R_{ν}^p are the distances from the center to the neutrino sphere. $R_{\text{mag}} = |\Delta Q_{\nu, B \neq 0}^+ / Q_{\nu, B=0}^+|$ is the maximum ratio of the neutrino heating rate contributed from the parity-violating effects, $\Delta Q_{\nu, B \neq 0}^+$ to the heating rate without the corrections, $Q_{\nu, B=0}^+$.

The configurations of the poloidal magnetic fields and the ratio of $\Delta Q_{\nu, B \neq 0}^+ / Q_{\nu, B=0}^+$ for some representative models at the final states are shown in Figure 6. In the models, whose initial profile of the rotation law and the magnetic field is cylindrical with high central concentration [the models with ‘‘CS(NU)’’ in the name], the shapes of the shock wave becomes very collimated near the rotational axis (see Fig. 1, *bottom left panel*). The final profile of the magnetic fields is also centrally concentrated with the strong magnetic fields ($B \sim 4 \times 10^{16}$ G), which is favorable for heating through parity-violating effects (see the top left and right panels of Fig. 6). As a result, the regions where the equatorial symmetry of the neutrino heating is broken become rather wider at the north and the south poles than in the other models, which have different initial profiles of the rotation and magnetic fields while the initial strength of rotation is fixed. If the initial strength of rotation is larger, the neutrino sphere is deformed and becomes more oblate owing to the centrifugal force (see the black region of the middle right panel of Fig. 6). Since the radii of the neutrino spheres tend to be smaller near the rotational axis than in the equatorial plane (see Table 3), the solid angle within which a point outside the neutrino sphere receives the rays from the neutrino sphere is enlarged for the vicinity of the rotational axis. This effect makes

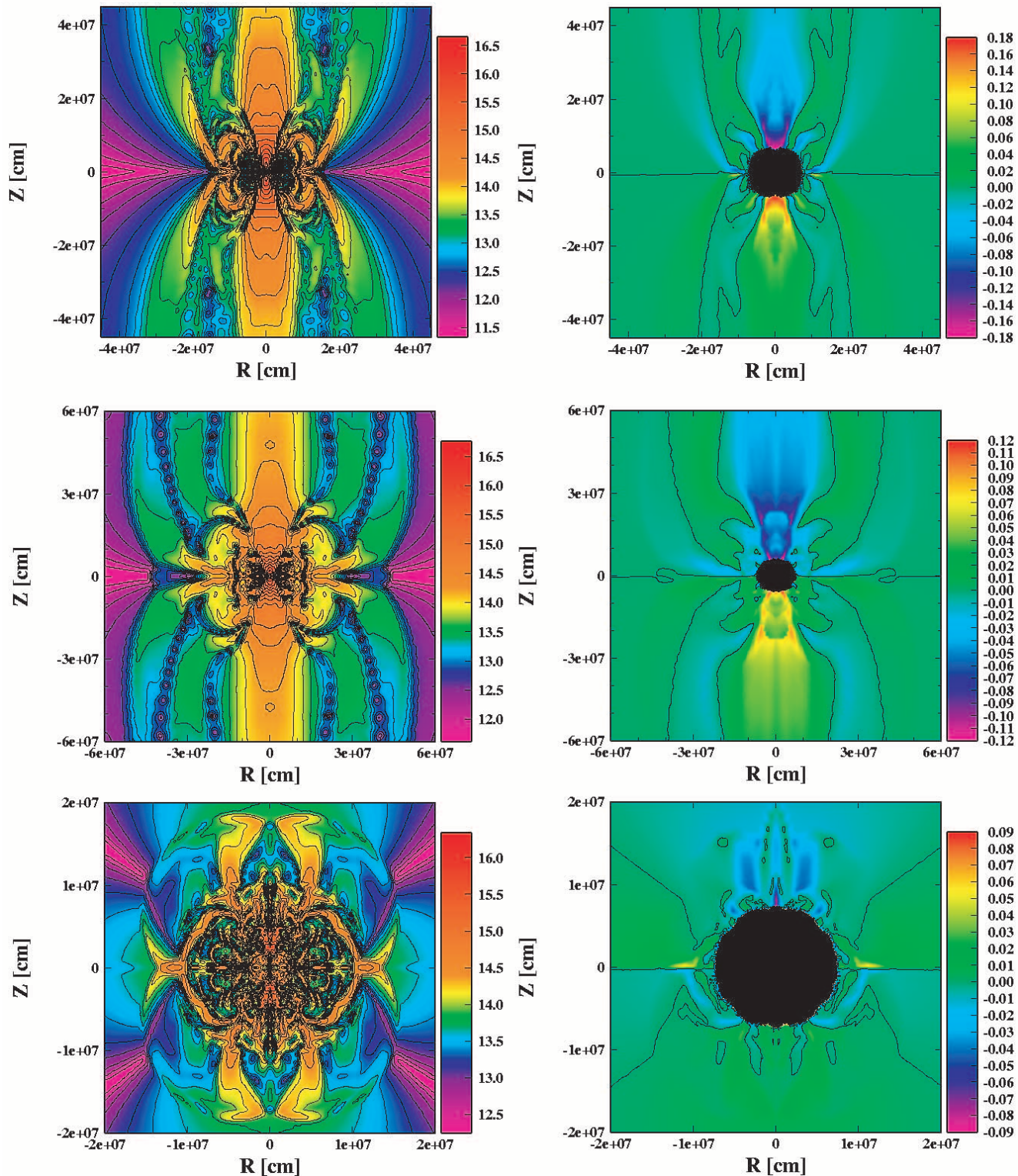


FIG. 6.—Contour of the logarithm of the poloidal magnetic fields (in gauss) (*left panels*) and the contour of $\Delta Q_{\nu, B \neq 0}^+ / Q_{\nu, B=0}^+$ in percentages (*right panels*). The top, middle, and bottom panels correspond to models CS(NU)-2, SS(NU)-1, and CS(Q)-2, respectively.

the neutrino heating near the rotational axis more efficient as in case of pure rotation (Kotake et al. 2003a). This rotation-induced anisotropic neutrino heating enhances the effect of the symmetry of the heating induced by the parity-violating corrections [see the values of R_{mag} in Table 3 and compare the values between the models with the same name except for the final number, for example, SL(U)-2 and SL(U)-1]. Furthermore, the regions that are heated asymmetrically are more en-

larged for the faster than for the slower rotating model (compare the top right and the middle right panels of Fig. 6).

Finally, we refer to the models whose initial profile of the magnetic field is quadrupole (see Fig. 6, *bottom panels*). In such models, there appear regions with strong magnetic fields which look like horns, near the rotational axis ranging from $\sim 100 \text{ km} < Z < 200 \text{ km}$ (see Fig. 6, *bottom left panel*). As a result, the heating regions influenced by the parity-violating

corrections become rather off-axis (see Fig. 6, *bottom right panel*).

4. DISCUSSION

In our computations, only electron neutrinos are treated approximately. Since all the numerical simulations are limited to rather early phases (~ 50 ms), it may not be a bad approximation. However, this becomes a certain limitation to the study at the later phases, which are more important for investigating the outcome of the north-south neutrino heating asymmetry discussed here. As already mentioned, if we take cooling into account, no heating region is found at these early times. As shown, for example, by Thompson et al. (2003), the heating region (or the gain region) appears more than 50–100 ms after core bounce. Hence, our estimate of anisotropic neutrino heating is admittedly a bold extrapolation to the later phases, which we have not computed yet.

As stated, multidimensional MHD simulations that solve the neutrino transport with parity-violating reactions are required in order to compute the relation between the asymmetric neutrino heating induced by the parity-violating corrections and the pulsar-kick. Although we hope that the general features obtained in this study will be adopted later on, further numerical investigations will be required to check the validity of our results.

As for the initial configurations of the poloidal magnetic fields, we assume that they have the same profile as the rotation. The assumption may not be unnatural because the angular momentum transfer in quasistatic stellar evolution is tightly connected to the formation of the magnetic fields (Parker 1979; Spruit 2002). However, multidimensional and self-consistent calculations need to be done to understand of the magneto-rotational evolution of supernova progenitors.

5. CONCLUSION

We performed a series of magnetohydrodynamic simulations of supernova cores. As for the microphysics, we employ a realistic equation of state based on the relativistic mean field theory and take into account electron captures and the neutrino transport via a neutrino leakage scheme. Since the profiles of the angular momentum and the magnetic fields of strongly magnetized stars are still quite uncertain, we constructed 11 initial models, changing the combination of the strength of the angular momentum, the rotations law, the degree of differential rotation, and the profiles of the magnetic fields in order to cover as wide a parametric freedom as possible. Based on numerical simulations, we estimated how rotation-induced anisotropic neutrino heating is changed by parity-violating corrections of neutrinos under strong magnetic fields. By so doing, we investigated the global asymmetry of the neutrino heating in a strongly magnetized supernova core. As a result, we found the following:

1. At the prompt-shock timescale (~ 50 ms after core bounce), the toroidal magnetic fields are formed mainly by the wrapping of the initial poloidal magnetic fields. The strength of the toroidal magnetic fields is smaller than the poloidal ones at this timescale. Although the growth timescale of MRI corresponding to the fastest growing mode of the instability is within the prompt-shock timescale, it is much longer than the growth of the wrapping timescale. The inefficiency of the growth of MRI is due to the initial slow rotation rates prior to core collapse, which reconciles with the results of the state-of-the-art stellar evolution calculations.

2. Whether the parity-violating corrections in the strong magnetic fields suppress or enhance the heating rate compared to

that without the corrections is found to be simply determined by the inner product of the unit vector of incoming neutrinos (\hat{n}) and the unit vector along the magnetic field direction (\hat{B}). In the models, except for those that initially have quadrupole magnetic fields, the poloidal magnetic fields near the rotational axis are almost aligned and parallel to the axis at the prompt-shock timescale. Although the neutrino emission is almost spherical in the slowly rotating models with the initial values of $T/|W| = 0.01\%$, the values of the inner product become positive in the regions as a result of the geometry of the magnetic field lines. This results in a reduction of the neutrino heating rates. In the faster rotating models with the initial value of $T/|W| = 0.1\%$, the rotation-induced anisotropic neutrino heating is found to enhance the asymmetric heating induced by the parity-violating correction more than in case of the slower rotating models. This is because the rotation-induced neutrino heating heats the regions near the rotational axis, where the magnetic fields are typically strongest, more efficiently. The ratio of the correction to the heating rate to the heating rate without the magnetic fields is found to range from 0.08% to 0.42%.

From the above results, we find that the neutrino heating rates are reduced by $\lesssim 0.5\%$ over those without the magnetic fields as a result of the parity-violating effects in the vicinity of the north pole of a star, while they are enhanced by about $\lesssim 0.5\%$ in the vicinity of the south pole. Based on these results, we speculate that the neutron star might be kicked toward the north pole in the subsequent period if the asymmetry of the neutrino heating in the north and the south poles develop in the later phases. This is because Scheck et al. (2004) recently pointed out that a random velocity perturbation with an amplitude of $\sim 0.1\%$ added artificially at several milliseconds after bounce can be the seed of global asymmetry of the supernova shock and the cause of the pulsar kick. In their models, the orientation of pulsar kicks depends stochastically on the initial random perturbation. This is the case for the observed pulsars with the canonical magnetic fields ($B \sim 10^{12}$ G). However, the asymmetry of the neutrino heating in the strong magnetic fields ($B \geq 10^{15}$ G) considered here might have influence on the alignment of spin and the space velocity of the pulsar associated with the formation of the magnetars. Although no pulsar kicks with very strong magnetic fields have been observed so far, the alignment of spin and the space velocity of the magnetars is expected to be observed by future observations.

As stated earlier, our simulations are crude in the treatment of microphysics compared with recent spherical models. This might be justified as long as we study the earlier phase in the prompt-explosion timescale. We are currently developing a two-dimensional neutrino transport code, which will be necessary to test the validity of implications obtained in this study (Kotake et al. 2004a).

K. K. is grateful to K. Sumiyoshi for providing us with the tabulated equation of state, which can be handled without difficulties, and to M. Shimizu for supporting computer environments. K. K. also thanks H. Sawai and T. Takiwaki for valuable discussions. The numerical calculations were partially done on the supercomputers at RIKEN and KEK (KEK supercomputer projects 02-87 and 03-92). This work was partially supported by Grants-in-Aid for the Scientific Research from the Ministry of Education, Science, and Culture of Japan through grants S 14102004, 14079202, and 14740166.

REFERENCES

- Akiyama, S., Wheeler, J. C., Meier, D. L., & Lichtenstadt, I. 2003, *ApJ*, 584, 954
- Ardeljan, N. V., Bisnovatyi-Kogan, G. S., & Moiseenko, S. G. 1998, in *IAU Colloq. 106, The Local Bubble and Beyond*, ed. D. Breitschwerdt, M. J. Freyberg, & J. Trümper (Berlin: Springer), 145
- . 2000, *A&A*, 355, 1181
- Arras, P., & Lai, D. 1999a, *ApJ*, 519, 745
- . 1999b, *Phys. Rev. D*, 60, 043001
- Arzoumanian, Z., Chernoff, D. F., & Cordes, J. M. 2002, *ApJ*, 568, 289
- Balbus, S. A., & Hawley, J. F. 1998, *Rev. Mod. Phys.*, 70, 1
- Bazan, G., & Arnett, D. 1998, *ApJ*, 496, 316
- Bisnovatyi-Kogan, G. S., & Ruzmaikin, A. A. 1976, *Ap&SS*, 42, 401
- Bludman, S. A., Lichtenstadt, I., & Hayden, G. 1982, *ApJ*, 261, 661
- Buras, R., Rampp, M., Janka, H.-T., & Kifonidis, K. 2003, *Phys. Rev. Lett.*, 90, 241101
- Burrows, A., & Hayes, J. 1996, *Phys. Rev. Lett.*, 76, 352
- Cordes, J. M., Wasserman, I., & Blaskiewicz, M. 1990, *ApJ*, 349, 546
- Duan, H., & Qian Y.-Z. *Phys. Rev. D* 2004, 69, 123004
- Epstein, R. I., & Pethick, C. J. 1981, *ApJ*, 243, 1003
- Fryer, C. L. 2004, *ApJ*, 601, L175
- Fryer, C. L., & Kalogera, V. 1997, *ApJ*, 489, 244
- Fryer, C. L., & Warren, M. S. 2004, *ApJ*, 601, 391
- Goldreich, P., Lai, D., & Sahrling, M. 1996, in *Unresolved Problems in Astrophysics*, ed. J. N. Bahcall, & J. P. Ostriker (Princeton: Princeton Univ. Press)
- Guseinov, O. H., Yazgan, E., Ankar, A., & Tagieva, S. O. 2003, *Int. J. Mod. Phys. D*, 1, 1
- Heger, A., Langer, N., & Woosley, S. E., *ApJ*, 2000, 528, 368
- Heger, A., Woosley, S. E., Langer, N., & Spruit, H. C. 2003, preprint (astro-ph/0301374)
- Helfand, D. J., Gotthelf, E. V., & Halpern, J. P. 2001, *ApJ*, 556, 380
- Horowitz, C. J., & Li, G. 1998, *Phys. Rev. Lett.*, 80, 3694
- Janka, H.-T., & Mueller, E. 1994, *A&A*, 290, 496
- Janka, H.-T., & Raffelt, G. G. 1999, *Phys. Rev. D*, 59, 023005
- Kaspi, V. M., et al. 1996, *Nature*, 381, 584
- Kotake, K., Ohnishi, N., Yamada, S., & Sato, K. 2004a, in preparation
- Kotake, K., Sawai, H., Yamada, S., & Sato, K. 2004b, *ApJ*, 608, 391
- Kotake, K., Yamada, S., & Sato, K. 2003a, *ApJ*, 595, 304
- . 2003b, *Phys. Rev. D*, 68, 044023
- Kotake, K., Yamada, S., Sato, K., Sumiyoshi, K., Ono, H., & Suzuki, H. 2004c, *Phys. Rev. D*, 69, 124004
- Lai, D. 2004, in *3D Signatures of Stellar Explosion*, ed. P. Kumar, C. Wheeler, & P. Höflic (Cambridge: Cambridge Univ. Press), in press
- Lai, D., Chernoff, D. F., & Cordes, J. M. 2001, *ApJ*, 549, 1111
- LeBlanc, J. M., & Wilson, J.R. 1970, *ApJ*, 161, 541
- Liebendörfer, M., Mezzacappa, A., Thiemann, F.-K., Messer, O. E. B., Hix, W. R., & Bruenn, S. W. 2001, *Phys. Rev. D*, 63, 103004
- Liebendörfer, M., Rampp, M., Janka, H.-T., & Mezzacappa, A. 2005, *ApJ*, in press
- Lorimer, D. R., Bailes, M., & Harrison, P. A. 1997, *MNRAS*, 289, 592
- Lyne, A. G., Lorimer, D. R. 1994, *Nature*, 369, 127
- Mirabel, I. F., Mignani, R., Rodrigues, I., Combi, J. A., Rodríguez, L. F., & Guglielmetti, F. 2002, *A&A*, 395, 595
- Müller, E., & Hillebrandt, W. 1979, *A&A*, 80, 147
- Müller, E., Rampp, M., Buras, R., Janka, H.-T., & Shoemaker, D. H. 2004, *ApJ*, 603, 221
- Ott, C. D., Burrows, A., Livne, E., & Walder, R. 2004, *ApJ*, 600, 834
- Parker, E. N. 1979, *Cosmological Magnetic Fields: Their Origin and Their Activity* (Oxford: Clarendon)
- Pavlov, G. G., Kargaltsev, O. Y., Sanwal, D., & Garmire, G. P. 2001, *ApJ*, 554, L189
- Rampp, M., & Janka, H.-T. 2000, *ApJ*, 539, L33
- Scheck, L., Plewa, T., Janka, H.-T., Kifonidis, K., & Müller, E. 2004, *Phys. Rev. Lett.*, 92, 011103
- Shen, H., Toki, H., Oyamatsu, K., & Sumiyoshi, K. 1998, *Nucl. Phys.*, A, 637, 43
- Spruit, H. C. 2002, *A&A*, 381, 923
- Stone, J. M., & Norman, M. L. 1992, *ApJS*, 80, 753
- Symbalisty, E. 1984, *ApJ*, 285, 729
- Takiwaki, T., Kotake, K., Nagataki, S., & Sato, K. 2004, *ApJ*, 616, 1086
- Thompson, T. A., Burrows, A., & Pinto, P. A. 2003, *ApJ*, 592, 434
- van Riper, K. A. 1982, *ApJ*, 257, 793
- van Riper, K. A., & Lattimer, J. M. 1981, *ApJ*, 249, 270
- Wex, N., Kalogera, V., & Kramer, M. 2000, *ApJ*, 528, 401
- Yamada, S., Kotake, K., & Yamasaki, T. 2004, *New. J. Phys.*, 6, 79
- Yamada, S., & Sawai, H. 2004, *ApJ*, 608, 907
- Zhang, B., & Harding, A. K. 2000, *ApJ*, 535, L51